Jyväskylän yliopiston julkaisuarkisto
Jyväskylä University Digital Archive

UNIVERSITY OF JYVÄSKYLÄ

This is an electronic reprint of the original article.
This reprint *may differ* from the original in pagination and typographic detail.

Author(s): Kostensalo, Joel; Haaranen, Mikko; Suhonen, Jouni

Title: Electron spectra in forbidden β decays and the quenching of the weak axial-vector coupling constant gA

Year: 2017

Version:

Please cite the original version:

Kostensalo, J., Haaranen, M., & Suhonen, J. (2017). Electron spectra in forbidden β decays and the quenching of the weak axial-vector coupling constant gA. Physical Review C, 95(4), Article 044313. https://doi.org/10.1103/PhysRevC.95.044313

All material supplied via JYX is protected by copyright and other intellectual property rights, and duplication or sale of all or part of any of the repository collections is not permitted, except that material may be duplicated by you for your research use or educational purposes in electronic or print form. You must obtain permission for any other use. Electronic or print copies may not be offered, whether for sale or otherwise to anyone who is not an authorised user.

Electron spectra in forbidden β decays and the quenching of the weak axial-vector coupling constant g_A

Joel Kostensalo,* Mikko Haaranen, and Jouni Suhonen†
Department of Physics, University of Jyvaskyla, P.O. Box 35, FI-40014, Finland
(Received 14 February 2017; published 12 April 2017)

Evolution of the electron spectra with the effective value of the weak axial-vector coupling constant $g_{\rm A}$ was followed for 26 first-, second-, third-, fourth- and fifth-forbidden β^- decays of odd-A nuclei by calculating the involved nuclear matrix elements (NMEs) in the framework of the microscopic quasiparticle-phonon model (MQPM). The next-to-leading-order terms were included in the β-decay shape factor of the electron spectra. The spectrum shapes of third- and fourth-forbidden nonunique decays were found to depend strongly on the value of $g_{\rm A}$, while first- and second-forbidden decays were mostly unaffected by the tuning of $g_{\rm A}$. The $g_{\rm A}$-driven evolution of the normalized β spectra was found to be quite universal, largely insensitive to the small changes in the nuclear mean field and the adopted residual many-body Hamiltonian producing the excitation spectra of the MQPM. This makes the comparison of experimental and theoretical electron spectra, coined "the spectrum-shape method" (SSM), a robust tool for extracting information on the effective values of the weak coupling constants. In this exploratory work two new experimentally interesting decays for the SSM treatment were discovered: the ground-state-to-ground-state decays of ^{99}Tc and ^{87}Rb. Comparing the experimental and theoretical spectra of these decays could shed light on the effective values of $g_{\rm A}$ and $g_{\rm V}$ for second- and third-forbidden nonunique decays. The measurable decay transitions of ^{135}Cs and ^{137}Cs, in turn, can be used to test the SSM in different many-body formalisms. The present work can also be considered as a (modest) step towards solving the $g_{\rm A}$ problem of the neutrinoless double beta decay.

DOI: 10.1103/PhysRevC.95.044313

I. INTRODUCTION

The observation of the neutrinoless mode of double beta decay ($0\nu\beta\beta$) would be groundbreaking since it would prove that the neutrino is its own antiparticle. The half-life of $0\nu\beta\beta$ decay is proportional to the fourth power of the weak axial-vector coupling constant $g_{\rm A}$ [1,2], but it is not quite clear what value to use for it when calculating theoretical predictions for the decay rates [3,4]. Theoretical predictions for the half-lives are crucial when designing optimal experimental setups to detect $0\nu\beta\beta$ events. In this context it is crucial to conceive complementary ways to address the $g_{\rm A}$ problem of $0\nu\beta\beta$ decay. One alternative is the study of β decays, both allowed and forbidden, since experimental data is available to compare with the calculated physical observables. The related quenching of the computed nuclear matrix elements (NMEs) was addressed already for the allowed Gamow–Teller [4] and first-forbidden [3] transitions in medium-heavy even-mass nuclei. In the present work we extend these studies to first-, second-, third-, fourth- and fifth-forbidden β^- decays of odd-mass (odd-A) nuclei by studying the shape evolution of the associated electron spectra and by calculating the involved nuclear matrix elements (NMEs) in the framework of the microscopic quasiparticle-phonon model (MQPM). In this way we hope to shed light on the effective value of $g_{\rm A}$ in forbidden β transitions, which play also a prominent role in the virtual transitions mediating the $0\nu\beta\beta$ decay.

The weak interaction is parity nonconserving, which is reflected in the fact that the hadronic current can be written as a mixture of vector and axial-vector components [5–7]. The weak coupling constants $g_{\rm V}$ and $g_{\rm A}$ appear in the theory of β decay as means to renormalize the hadronic current, when moving from the quark level to nucleons [8]. The conserved vector-current hypothesis (CVC) and the partially conserved axial-vector-current hypothesis (PCAC) of the standard model can be used to derive the free-nucleon values $g_{\rm V} = 1.00$ and $g_{\rm A} = 1.27$ [9]. In nuclear matter, however, the value of $g_{\rm A}$ is affected by many-nucleon correlations, and so in practical calculations a quenched effective value could give results which are closer to experimental results [10]. In the practical calculations the shortcomings in the treatment of the many-body quantum mechanics could also be absorbed into the value of $g_{\rm A}$ [11,12].

In earlier studies the effective value of the weak axial-vector coupling constant was probed by comparing the experimental half-lives of Gamow–Teller and first-forbidden unique decays to those predicted by the proton-neutron quasiparticle random-phase approximation (pnQRPA) [3,4,13–15]. These studies show consistently that a quenched value of $g_{\rm A}$ is needed to reproduce the experimental data. In Ref. [16] a systematic study of high-forbidden unique decays showed similar features as the earlier studies supporting the fact that a quenched effective value of $g_{\rm A}$ might need to be used for the high-forbidden decay branches as well.

In a recent study (see Ref. [17]) an interesting new feature was found regarding the weak coupling constants $g_{\rm V}$ and $g_{\rm A}$. The shape of the electron spectra of the fourth-forbidden nonunique ground-state-to-ground-state β^- decays of ^{113}Cd and ^{115}In depend strongly on the value of $g_{\rm V}$ and $g_{\rm A}$ due to

*joel.j.kostensalo@student.jyu.fi
†jouni.suhonen@phys.jyu.fi

 ©2017 American Physical Society

TABLE I. Change in angular momentum ΔJ and parity π in a Kth forbidden β decay. The decays with $\Delta J = K$ (in the case of $K = 1$ also $\Delta J = 0$) are known as nonunique, while those with $\Delta = K + 1$ are known as unique.

K	1	2	3	4	5
ΔJ	0,1,2	2,3	3,4	4,5	5,6
$\pi_i\pi_f$	-1	$+1$	-1	$+1$	-1

the complicated shape factor featuring vector, axial-vector, and mixed vector-axial-vector parts containing a number of different NMEs and phase-space factors. The shapes of the theoretical and experimental spectra can be compared to find the effective values of the coupling constants in a new method called the spectrum-shape method (SSM). The study [17] used two nuclear models; namely, the MQPM [18,19] and the nuclear shell model (NSM) [20–22]. When the computed electron spectra of ^{113}Cd were compared with the experimental spectrum of Ref. [23], a close match was found by using the effective values $g_A \approx 0.90$ and $g_V = 1.0$ (equal to its CVC value!). This study was extended in Ref. [24] to include also the NMEs calculated within the microscopic interacting boson-fermion model (IBFM-2) [25,26]. The remarkable result of this study was that the three models MQPM, NSM, and IBFM-2 yielded a consistent result of $g_A \approx 0.92$ by comparison with the experimental electron spectrum of Ref. [23]. This is the more surprising when considering the very different theory frameworks of the three models. The qualitative behavior of the MQPM, NSM, and IBFM-2 spectra was remarkably similar for both the ^{113}Cd and ^{115}In decays, suggesting that the details of the nuclear residual Hamiltonian and the many-body methods to solve the associated eigenvalue problem do not affect much the the evolution of the electron spectra and thus the SSM itself. Based on this, it is reasonable to conjecture that just one of these models could be used to further explore new, potentially interesting β decays and their basic features.

In this paper we set out to find if the β spectra of other forbidden decays depend sensitively on the value of g_A using the MQPM, which can be relatively easily applied to a large number of odd-A nuclei. We will explore unique and nonunique first- and second-forbidden decays and third-, fourth-, and fifth-forbidden nonunique decays. The identification of the degree of forbiddeness of a β-decay transition is presented in Table I. Most of these transitions and the associated electron spectra can be measured in the present and future low-background (underground) experiments. Some of the considered higher-forbidden transitions, with competing allowed transitions, cannot be easily measured. They were, however, included to better access the possible systematic features in transitions of increasing forbiddeness. As in Refs. [17] and [24] we take into account the next-to-leading-order terms in the shape factor, and so the spectra of unique-forbidden decays also depend on the axial-vector coupling constant in a nontrivial way. Based on the conclusions of Ref. [17], we adopt the CVC value $g_V = 1.00$ in the calculations. In the analyzes we use the normalized electron spectra (the normalized spectra are also used when comparing with available experimental data) for which the integrated area under the spectrum curve is unity. While the half-life is affected by the absolute values of the weak coupling constants, the normalized electron spectra depend only on the ratio g_A/g_V, so varying only g_A is sufficient.

The microscopic quasiparticle-phonon model is a fully microscopic model, which can be used to describe spherical and nearly spherical open-shell odd-A nuclei. In the MQPM all three parts of the Hamiltonian, namely the quasiparticle, phonon, and quasiparticle-phonon terms are treated in an internally consistent way. The odd-A nucleus is built from a basis of one- and three-quasiparticle states. The one-quasiparticle states are obtained by performing a BCS calculation for the neighboring even-even reference nucleus, and the three-quasiparticle states by coupling the BCS quasiparticles to the QRPA phonons of Ref. [18]. Finally, the residual Hamiltonian, which contains the interaction of the odd nucleon and the even-even reference nucleus, is diagonalized in the combined one- and three-quasiparticle basis [19].

This article is organized as follows: In Sec. II we give the theoretical background behind the MQPM and the β spectrum shape. In Sec. III we describe the application of the MQPM to the spectrum shape of forbidden β^- decays. In Sec. IV we present our results, and in Sec. V we draw the conclusions.

II. THEORETICAL FORMALISM

In this section we give the theoretical background behind the nuclear model MQPM used in the calculations (see Sec. II A) and present the practical aspects of the theory of forbidden β^- decays and the shape of the electron spectra (see Sec. II B). The description of the MQPM summarizes the two original papers describing the model (see Refs. [18] and [19]). For a more complete description of the theory of β decays, see Ref. [27].

A. Microscopic quasiparticle-phonon model

The starting point of the MQPM is a realistic A-fermion Hamiltonian consisting of the mean-field part and the residual-interaction part. In the occupation-number representation the Hamiltonian reads [10]

$$H = \sum_{\alpha} \epsilon_\alpha c_\alpha^\dagger c_\alpha + \frac{1}{4} \sum_{\alpha\beta\gamma\delta} \bar{v}_{\alpha\beta\gamma\delta} c_\alpha^\dagger c_\beta^\dagger c_\delta c_\gamma, \tag{1}$$

where $c_\iota^\dagger$ and c_ι are the creation and annihilation operators of the Hartree–Fock quasiparticles and $\bar{v}_{\alpha\beta\gamma\delta} = \langle\alpha\beta|v|\gamma\delta\rangle - \langle\alpha\beta|v|\delta\gamma\rangle$ is the antisymmetrized two-body matrix element. Here we adopt the notation of Baranger [28], where the Roman letter a includes the single-particle quantum numbers n_a (principal), l_a (orbital angular momentum), and j_a (total angular momentum) and the Greek letter α, the quantum numbers a, and the magnetic quantum number m_a.

The approximate ground state of the even-even reference nucleus is obtained by using BCS theory [29]. The occupation and vacancy amplitudes v_a and u_a emerge from the Bogoliubov–Valatin transformation [30,31],

$$a_\alpha^\dagger = u_a c_\alpha^\dagger + v_a \tilde{c}_\alpha, \tag{2}$$

$$\tilde{a}_\alpha = u_a \tilde{c}_\alpha - v_a c_\alpha^\dagger, \tag{3}$$

where $a^\dagger_\alpha$ is the BCS quasiparticle creation operator and $\tilde{a}_\alpha$ is the time-reversed BCS quasiparticle annihilation operator. After the Bogoliubov–Valatin transformation, the Hamiltonian of Eq. (1) can be written as

$$H = H_{11} + H_{22} + H_{40} + H_{04} + H_{31} + H_{13}, \tag{4}$$

where the indices correspond to the number of BCS creation and annihilation operators [32]. The terms H_{20} and H_{02} are missing from Eq. (4), since they vanish when minimizing the BCS ground-state energy.

When solving the BCS equations (see formulation in, e.g., Ref. [10]), the monopole matrix elements of the two-body interaction can be scaled by pairing-strength parameters $g^{(\mathrm{n})}_{\mathrm{pair}}$ and $g^{(\mathrm{p})}_{\mathrm{pair}}$ to reproduce the semi-empirical pairing gaps. The proton and neutron pairing gaps Δ_p and Δ_n needed for solving the BCS equations can be calculated by using the three-point formulas [33,34],

$$\begin{aligned}\Delta_\mathrm{p}(A,Z) &= \tfrac{1}{4}(-1)^{Z+1}[S_\mathrm{p}(A+1,Z+1)\\ &\quad - 2S_\mathrm{p}(A,Z) + S_\mathrm{p}(A-1,Z-1)],\\ \Delta_\mathrm{n}(A,Z) &= \tfrac{1}{4}(-1)^{A-Z+1}[S_\mathrm{n}(A+1,Z)\\ &\quad - 2S_\mathrm{n}(A,Z) + S_\mathrm{n}(A-1,Z)],\end{aligned} \tag{5}$$

where S_p is the proton separation energy and S_n the neutron separation energy.

Once the one-quasiparticle states have been calculated by using BCS theory, the next step is to consider two-quasiparticle excitations, i.e., treat the H_{22}, H_{40}, and H_{04} terms of the Hamiltonian (4). In the MQPM, the two-quasiparticle excitations are the quasiparticle random-phase approximation (QRPA) [28] phonons of the even-even reference nucleus defined by the QRPA phonon-creation operator

$$Q^\dagger_\omega = \sum_{a\leqslant a'} \left[X^\omega_{aa'} A^\dagger_{aa'}(J_\omega M) - Y^\omega_{aa'} \tilde{A}_{aa'}(J_\omega M)\right], \tag{6}$$

where ω denotes the angular momentum J_ω, parity π_ω, and the index k_ω which identifies the different excitations with the same J and π. The quantity $A^\dagger_{aa'}(J_\omega M) = (1+\delta_{aa'})^{-1/2}$ $[a^\dagger_a a^\dagger_{a'}]_{J_\omega}$ is the two-quasiparticle creation operator, and $\tilde{A}_{aa'}(J_\omega M) = (1+\delta_{aa'})^{-1/2}[\tilde{a}_a \tilde{a}_{a'}]_{J_\omega}$ is the corresponding annihilation operator. The forward- and backward-going amplitudes X and Y are solved by diagonalizing the QRPA matrix (see, e.g., Ref. [10]).

The basis states of the microscopic quasiparticle-phonon model are the one-quasiparticle states given by the BCS calculation and the three-quasiparticle states emerging from the coupling of QRPA phonons with BCS quasiparticles. The states of the odd-A nucleus are created by the MQPM creation operator [19]

$$\Gamma^\dagger_i(jm) = \sum_n C^i_n a^\dagger_{njm} + \sum_{a\omega} D^i_{a\omega}[a^\dagger_a Q^\dagger_\omega]_{jm}, \tag{7}$$

where C^i_n and $D^i_{a\omega}$ are the amplitudes determined by the MQPM matrix equation. The use of the equations-of-motion method [35] leads to the generalized eigenvalue problem [18]

$$\begin{pmatrix} A & B \\ B^T & A' \end{pmatrix}\begin{pmatrix} C^i \\ D^i \end{pmatrix} = \Omega_i \begin{pmatrix} 1 & 0 \\ 0 & N \end{pmatrix}\begin{pmatrix} C^i \\ D^i \end{pmatrix}, \tag{8}$$

where the submatrices A, A', and B are the matrix elements of H_{11}, H_{22}, and H_{31} of equation (4), respectively. The explicit expressions for these submatrices are listed in Ref. [19]. The overlap between a one-quasiparticle state and a three-quasiparticle state is always zero leading to a block-diagonal structure of the overlap matrix on the right-hand side of Eq. (8). The overlaps between one-quasiparticle states lead to the unity matrix and the overlaps between three-quasiparticle states lead to the submatrix N of the overlap matrix. The appearance of the nondiagonal submatrix N in the overlap matrix leads, in turn, to a non-Hermitian eigenvalue problem in a nonorthogonal, often over-complete, basis set.

To solve the non-Hermitian eigenvalue problem of Eq. (8), we turn it into a Hermitian problem by writing it in a new orthogonal basis and diagonalizing it in the usual way. We start by solving the eigenvalue problem of the overlap matrix N, which reads

$$\sum_j N_{ij} u^{(k)}_j = n_k u^{(k)}_i. \tag{9}$$

The eigenvectors of N can be written in the basis $|i\rangle = \Gamma^\dagger_i |\mathrm{QRPA}\rangle$, where $|\mathrm{QRPA}\rangle$ is the correlated ground state of the reference nucleus, as [19]

$$|\tilde{k}\rangle = \frac{1}{\sqrt{n_k}} \sum_i u^{(k)}_i |i\rangle\,. \tag{10}$$

The states $|\tilde{k}\rangle$ with a nonzero eigenvalue n_k form an orthonormal complete set. In the orthonormal basis of Eq. (10) the MQPM matrix equation (8) can be written as a real and symmetric eigenvalue problem,

$$\sum_l \langle\tilde{k}|H|\tilde{l}\rangle g^{(n)}_l = \lambda_n g^{(n)}_k, \tag{11}$$

where

$$\langle\tilde{k}|H|\tilde{l}\rangle = \frac{1}{\sqrt{n_k n_l}} \sum_{ij} u^{(k)*}_i \langle i|H|j\rangle u^{(l)}_j. \tag{12}$$

The coefficients C^n_i of the MQPM matrix equation can be calculated from the coefficients g using the equation [19]

$$C^n_i = \sum_k \frac{1}{\sqrt{n_k}} g^{(n)}_k u^{(k)}_i. \tag{13}$$

As an example of the kind of excitation spectrum that the microscopic quasiparticle-phonon model produces, the experimental and MQPM spectra of ^{87}Sr are presented in Fig. 1. The experimental spectrum was obtained from Ref. [36].

B. β spectrum shape

To simplify the description of the β^- decay, we assume that at the very moment of decay the decaying nucleus only interacts via the weak interaction, and the strong interaction with the $A-1$ other nucleons can be neglected. In this scheme, known as the impulse approximation, the flow lines of the nucleons, i.e., the hadronic current, and the flow lines of the emitted leptons, i.e., the leptonic current, interact at a weak-interaction vertex. Since the vector boson W^- has a large mass, and thus propagates only a short distance, the vertex

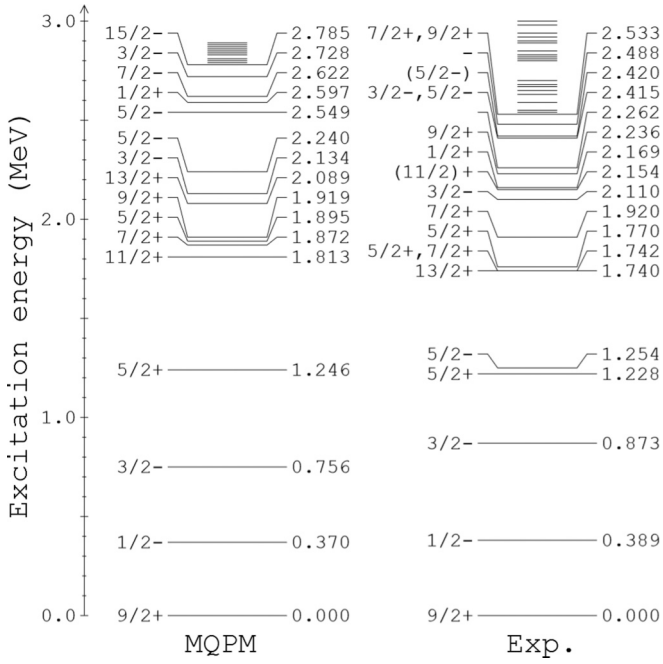

FIG. 1. Experimental and MQPM excitation spectra for the nucleus ^{87}Sr.

can be considered to be point like with an effective coupling constant G_{F}, the Fermi constant. The weak interaction is parity nonconserving, which is reflected in the fact that the hadronic current can be written at the quark level as a mixture of vector and axial-vector components as [5–7]

$$J_H^{\mu} = \bar{u}(x)\gamma^{\mu}(1-\gamma_5)d(x), \tag{14}$$

where γ^{μ} and γ_5 are the usual Dirac matrices. When moving from the quark level to the nucleon level, one must take into account renormalization effects of strong interactions. The hadronic current at the nucleon level (proton p and neutron n) can then be written as [8]

$$J_H^{\mu} = \bar{p}(x)\gamma^{\mu}(g_{\mathrm{V}} - g_{\mathrm{A}}\gamma_5)n(x), \tag{15}$$

where g_{V} and g_{A} are the weak vector and axial-vector coupling constants, respectively. The conserved vector-current hypothesis (CVC) and the partially conserved axial-vector-current hypothesis (PCAC) of the standard model give the so-called bare nucleon values $g_{\mathrm{V}} = 1.0$ and $g_{\mathrm{A}} = 1.27$ [9]. In nuclear matter the value of g_{A} is affected by many-nucleon correlations, and so the bare nucleon value might not be the one to use in practical calculations [10].

In the impulse approximation the probability of the electron being emitted with kinetic energy between W_e and $W_e + dW_e$ is

$$P(W_e)dW_e = \frac{G_{\mathrm{F}}}{(\hbar c)^6}\frac{1}{2\pi^3\hbar}C(W_e)p_e c W_e(W_0 - W_e)^2 \times F_0(Z,W_e)dW_e, \tag{16}$$

where p_e is the momentum of the electron, Z is the proton number, $F_0(Z,W_e)$ is the Fermi function, and W_0 is the endpoint energy of the β spectrum. The shape factor $C(w_e)$ encodes the nuclear-structure information.

The half-life of a β decay can be expressed as

$$t_{1/2} = \frac{\kappa}{\tilde{C}}, \tag{17}$$

where $\tilde{C}$ is the integrated shape factor and κ is a constant with value [37]

$$\kappa = \frac{2\pi^3\hbar^7 \ln 2}{m_e^5 c^4 (G_{\mathrm{F}}\cos\theta_{\mathrm{C}})^2} = 6147\ \mathrm{s}, \tag{18}$$

with θ_{C} being the Cabibbo angle. For convenience, it is common to introduce unitless kinematic quantities $w_e = W_e/m_e c^2$, $w_0 = W_0/m_e c^2$, and $p = p_e c/(m_e c^2) = (w_e^2 - 1)^{1/2}$. Using these quantities the integrated shape factor can be written as

$$\tilde{C} = \int_1^{w_0} C(w_e)p w_e(w_0 - w_e)^2 F_0(Z,w_e)dw_e. \tag{19}$$

In Eq. (19) the kinematic factors are universal and the shape factor $C(w_e)$ has a complicated expression including both kinematic and nuclear form factors. The choice of nuclear model (in the case of this paper, MQPM) enters the picture when calculating the one-body transition densities [38] related to the NMEs of the shape factor. The details of the shape factor and the constitution of its NMEs can be found from Refs. [27] and [38]. As in the Refs. [17] and [24] we take into account the next-to-leading-order terms of the shape function (for details see Ref. [24]). In the commonly adopted leading-order approximation the shape of the electron spectrum of unique-forbidden decays does not depend on the NMEs and it is just scaled by g_{A}^2. When the next-order terms are taken into account, the shape factor of these decays depends on the computed NMEs and through this on g_{A} in a nontrivial way [24]. This means that, at least in theory, the SSM could be applied also to unique decays.

The shape factor $C(w_e)$ can be decomposed into vector, axial-vector, and vector-axial-vector parts. In this decomposition the shape factor reads

$$C(w_e) = g_{\mathrm{V}}^2 C_{\mathrm{V}}(w_e) + g_{\mathrm{A}}^2 C_{\mathrm{A}}(w_e) + g_{\mathrm{V}} g_{\mathrm{A}} C_{\mathrm{VA}}(w_e). \tag{20}$$

For the integrated shape factor we get the analogous expression

$$\tilde{C} = g_{\mathrm{V}}^2 \tilde{C}_{\mathrm{V}} + g_{\mathrm{A}}^2 \tilde{C}_{\mathrm{A}} + g_{\mathrm{V}} g_{\mathrm{A}} \tilde{C}_{\mathrm{VA}}. \tag{21}$$

In should be noted that in Eq. (20) the shape factors C_i are functions of electron kinetic energy, while the integrated shape factors $\tilde{C}_i$ in Eq. (21) are real numbers.

III. NUMERICAL APPLICATION OF FORMALISM

The electron spectra of 26 forbidden β^- transitions were calculated for different values of the coupling constants g_{A} by using the NMEs produced by the MQPM model. The application of the MQPM model followed the same basic steps as the earlier studies regarding the fourth-forbidden nonunique ground-state-to-ground-state β^- decays of ^{113}Cd, ^{115}In [17,24,38], and ^{115}Cd [39], including the use of the Bonn one-boson exchange potential with G-matrix techniques [19].

The single-particle energies needed to solve the BCS equations were calculated by using the Coulomb-corrected

Woods–Saxon potential with the Bohr–Mottelson parametrization [40]. For the protons of the even-even reference nuclei the valence space spanned 10 single-particle states in the range $0f_{7/2}$–$0h_{11/2}$. This valence space was also used for the neutrons of the reference nuclei with $A < 90$, while for the heavier nuclei a larger valence space spanning the single-particle-orbitals $0f_{5/2}$–$0i_{13/2}$ (15 single-particle states) was used.

The BCS one-quasiparticle spectra were tuned by adjusting manually some of the key single-particle energies computed by using the Woods–Saxon potential. This was done to get a closer mach between the low-lying one-quasiparticle states and the measured experimental ones. The adjustments were kept minimal with some changes in the span of spin-orbit gap(s) close to the proton and/or neutron Fermi surfaces. The computed pairing gaps were adjusted to fit the empirical values by tuning the pairing strength parameters $g^p_{\rm pair}$ and $g^n_{\rm pair}$ for protons and neutrons, separately. The empirical values were calculated by using the three-point formulas (5) and the experimental separation energies given in Ref. [41]. The QRPA spectra of the reference nuclei were tuned by scaling the particle-hole matrix elements with the parameter $g_{\rm ph}$ in order to reproduce the excitation energy of the lowest state of a given multipolarity. In the MQPM calculations a 3.0 MeV cutoff energy was used for the QRPA phonons to decrease the formidable computational burden.

IV. RESULTS AND DISCUSSION

Below we present our results: the electron spectra of 26 forbidden β^- decays (Figs. 2–9) and their integrated shape factors (Table II). The electron spectra are discussed in Sec. IV A and the integrated shape factors in Sec. IV B.

A. Electron spectra and effective value of $g_{\rm A}$

The electron spectra for the studied first-forbidden decays are presented in Figs. 2–4 for $g_{\rm A} = 0.80$–1.20 (the identification of the decay type is presented in Table I). Similar figures for second-, third-, fourth-, and fifth-forbidden decays are presented in Figs. 5–9.

For the nonunique decay of ^{125}Sb, presented in Fig. 2(a), decreasing the value of $g_{\rm A}$ increases the intensity of electrons emitted with low energies (0–100 keV), while decreasing the intensity of electrons with energies 250–350 keV. The differences in the shapes of the spectra are however very small—nothing like the dramatic behavior observed for the fourth-forbidden decays of ^{113}Cd and ^{115}In in Refs. [17] and [24]. From the other first-forbidden decays very slight changes in the low-energy spectrum can be seen for the nonunique decays of ^{141}Ce in Fig. 2(b) and ^{169}Er in Fig. 3(a), as well as for the unique decay of ^{79}Se below it in Fig. 3(b). For the other first-forbidden decays the β spectrum seems to be independent of the value of $g_{\rm A}$. The slight variation in the spectrum of ^{79}Se can only be seen when the next-to-leading-order terms of the shape factor are taken into account. In the lowest-order approximation the spectrum would be completely unaffected when $g_{\rm A}$ is varied. The variation is minimal, but on the other hand, it is also minimal for the nonunique first-forbidden decays.

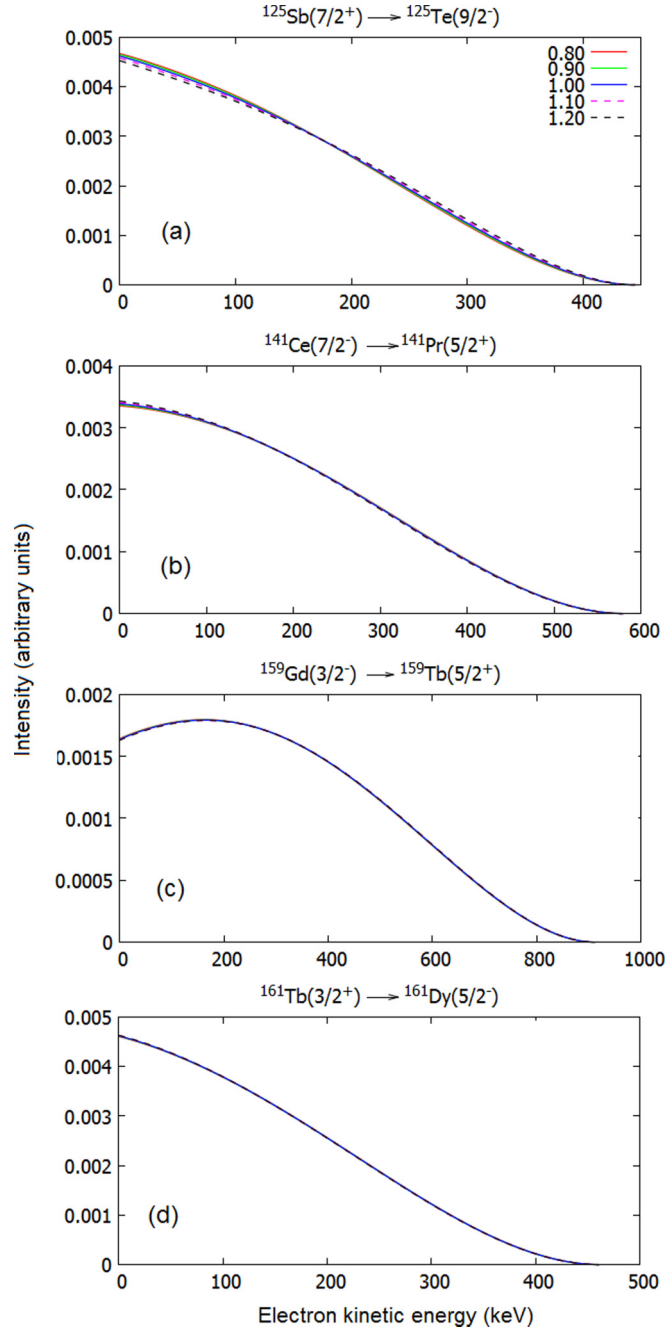

FIG. 2. The β spectra for first-forbidden nonunique β^- decays of the ground states of ^{125}Sb, ^{141}Ce, ^{159}Gd, and ^{161}Tb. The color coding represents the value of the weak axial-vector coupling constant $g_{\rm A}$. For the vector coupling constant $g_{\rm V}$ the value 1.00 was adopted.

Another interesting feature for the first-forbidden decays is the remarkably similar shapes of the ^{125}Sb, ^{141}Ce, ^{161}Tb [Figs. 2(a), 2(b), and 2(d)], ^{169}Er, ^{79}Se [Figs. 3(a) and 3(b)], and ^{107}Pd [Fig. 4(a)] spectra. For all of these the spectrum shape can be described as linearly decreasing with a slight downward bend at approximately 75% of the Q value. This is remarkable, since the Q values vary from a tiny 34.1(23) keV for ^{107}Pd to a much larger 580.4(11) keV for ^{141}Ce [36]. Another group of decays with very similar spectra are the first-forbidden unique

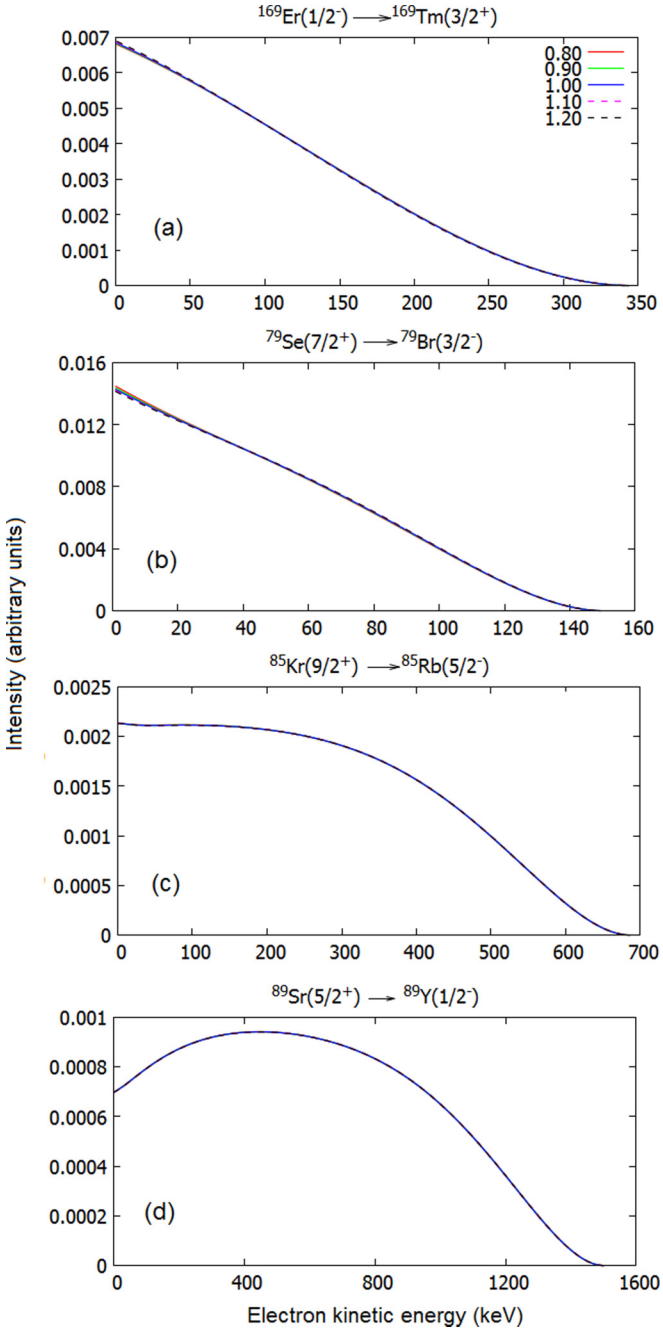

FIG. 3. The same as Fig. 2, but for the first-forbidden nonunique decay of ^{169}Er and the unique decays of ^{79}Se, ^{85}Kr, and ^{89}Sr.

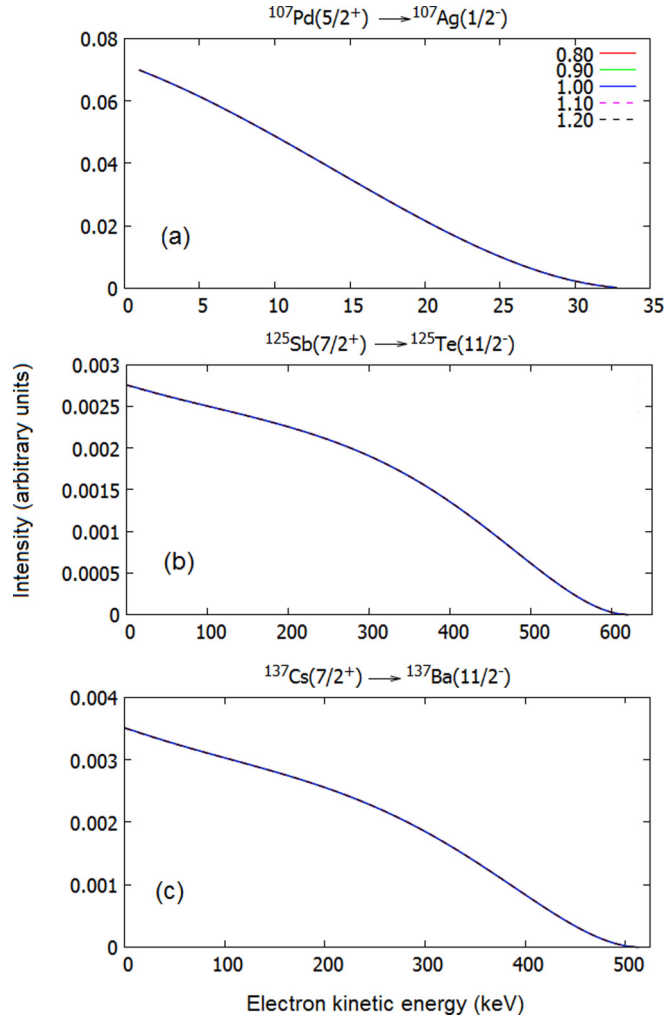

FIG. 4. The same as Fig. 2, but for the first-forbidden unique decays of ^{107}Pd, ^{125}Sb, and ^{137}Cs.

decay of ^{125}Sb and ^{137}Cs to the isomeric $11/2^-$ states of the daughter nuclei presented in Figs. 4(b) and 4(c) and the second-forbidden unique decay of ^{129}I shown in Fig. 5(a). Common to this group of decays is that the initial state has spin-parity $7/2^+$. For the decays of the first group no such obvious common feature is seen.

The electron spectra of second-forbidden decays shown in Fig. 5 differ from each other much more than the first-forbidden ones. In the case of the second-forbidden unique decay of ^{129}I the next-to-leading-order terms of the shape factor do not make the beta spectrum, shown in Fig. 5(a), dependent on g_A in a noticeable way. Slight bending is seen for the nonunique decay of ^{93}Zr [Fig. 5(b)], but the only second-forbidden transition showing heavy g_A dependence is the ground-state-to-ground-state decay of ^{99}Tc presented in Fig. 5(c). The dependence is similar to that observed in Refs. [17,24] for ^{113}Cd and ^{115}In: when $g_A \approx g_V$ a bell-shaped spectrum is produced, while otherwise the spectrum is monotonically decreasing. This decay is an excellent candidate for SSM. Comparison with experimental spectra could shed light on the effective value of g_A for second-forbidden nonunique transitions, and even second-forbidden β decays in general. The shape of ^{135}Cs and ^{137}Cs spectra on the other hand does not depend on the value of axial-vector coupling constant at all, as seen from Figs. 5(d) and 5(e). Decays such as the ground-state-to-ground-state decays of ^{135,137}Cs, which are practically independent of g_A, are also experimentally important, since they could be used to check the accuracy of the theoretical spectra predicted by the MQPM as well as by other nuclear models, such as the nuclear shell model and the microscopic interacting boson-fermion model.

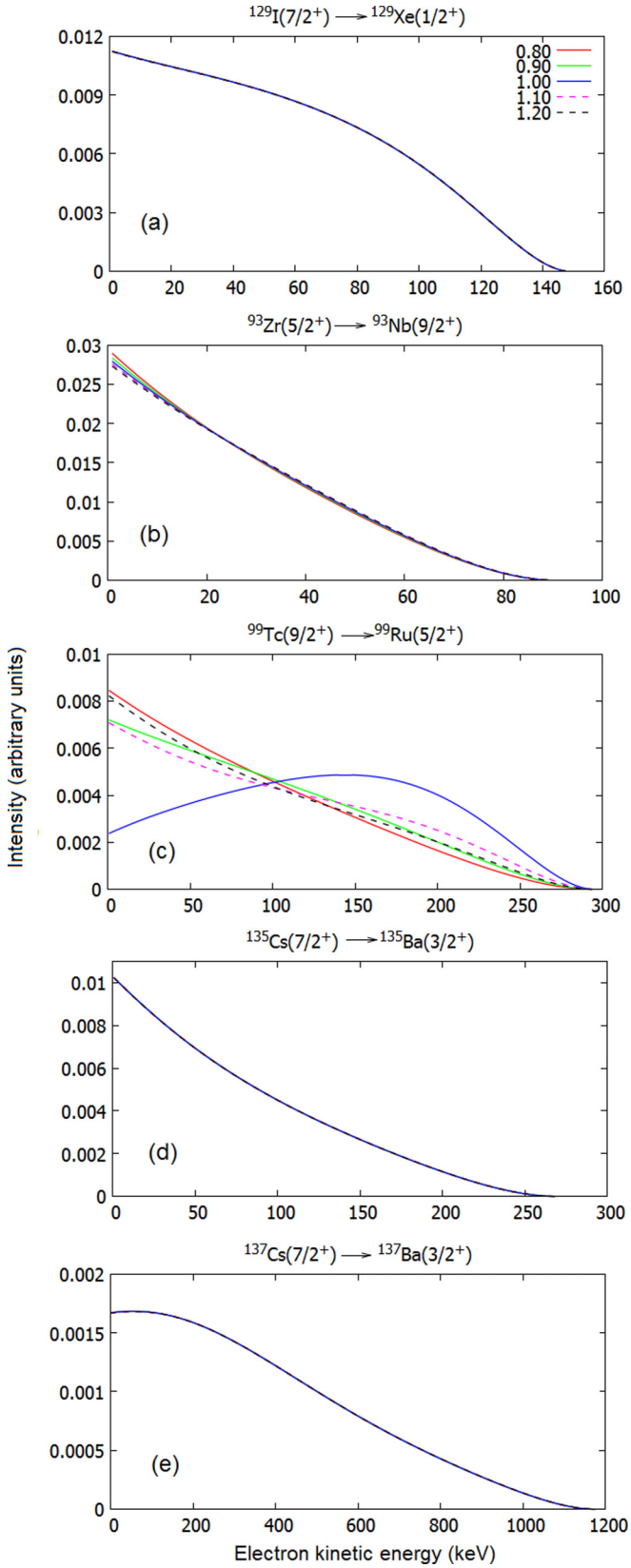

FIG. 5. The same as Fig. 2, but for the second-forbidden unique decay of ^{129}I and the nonunique decays of ^{93}Zr, ^{99}Tc, ^{135}Cs, and ^{137}Cs.

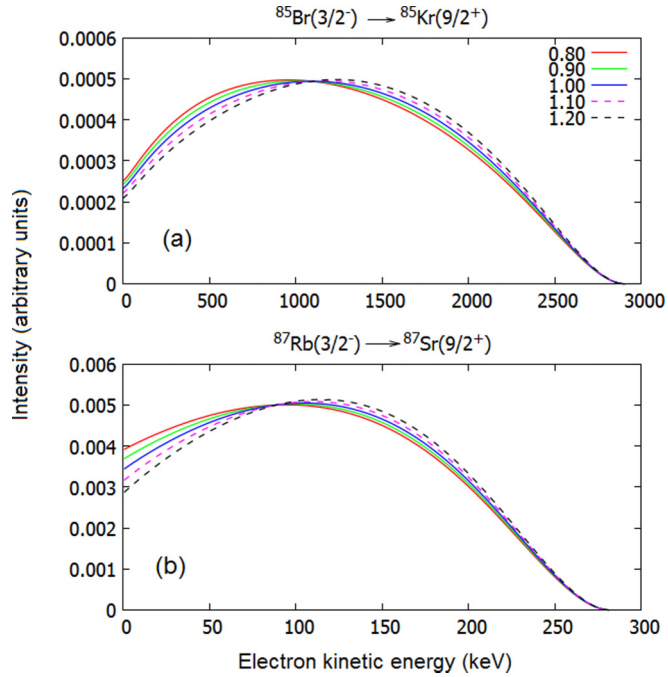

FIG. 6. The same as Fig. 2, but for the third-forbidden nonunique decays of ^{85}Br and ^{87}Rb.

While doing the MQPM calculation for the ^{137}Cs decay, an important new feature of the β spectra was discovered. While the area under the curve depends significantly on the computed MQPM level scheme (e.g., the one shown in Fig. 1), the shape of the normalized (to unit area) electron spectrum does not. Even shifting the single-particle energies enough to change the ordering of energy levels in the odd-A nucleus did not change the shape of the normalized spectrum at all. The other studied nuclei behave similarly, although for some of them slight changes in the electron spectrum were seen. At the mean-field level, moving arbitrarily the key single-particle orbitals at the proton and/or neutron Fermi surfaces by 0.5–1.5 MeV had very little effect. However, the shape is not completely independent of the computed level scheme, and large changes in it can deform the electron spectrum considerably. In terms of practical calculations it appears that getting the low end of the level scheme to reasonably agree with data, with the right ground-state spin-parity and few low-lying states near their experimental counterparts, is sufficient to produce an electron spectrum which is largely unaffected by further fine tuning. On the other hand, the theoretical half-life predictions can change by orders of magnitude when small changes to the single-particle energies are made, especially in cases where the even-even reference nucleus is (semi-)magic [16]. This stems from the sharp Fermi surface and vanishing pairing gap, making the BCS-approach sensitive to the details of the single-particle spectrum at the Fermi surface.

The results for third-forbidden nonunique ground-state-to-ground-state decays of ^{85}Br and ^{87}Rb are shown in Fig. 6. The shape factor depends on g_A in a very similar manner, even though the Q value for ^{85}Br is tenfold larger than the one for ^{87}Rb. Both of these decays are from a $3/2^-$

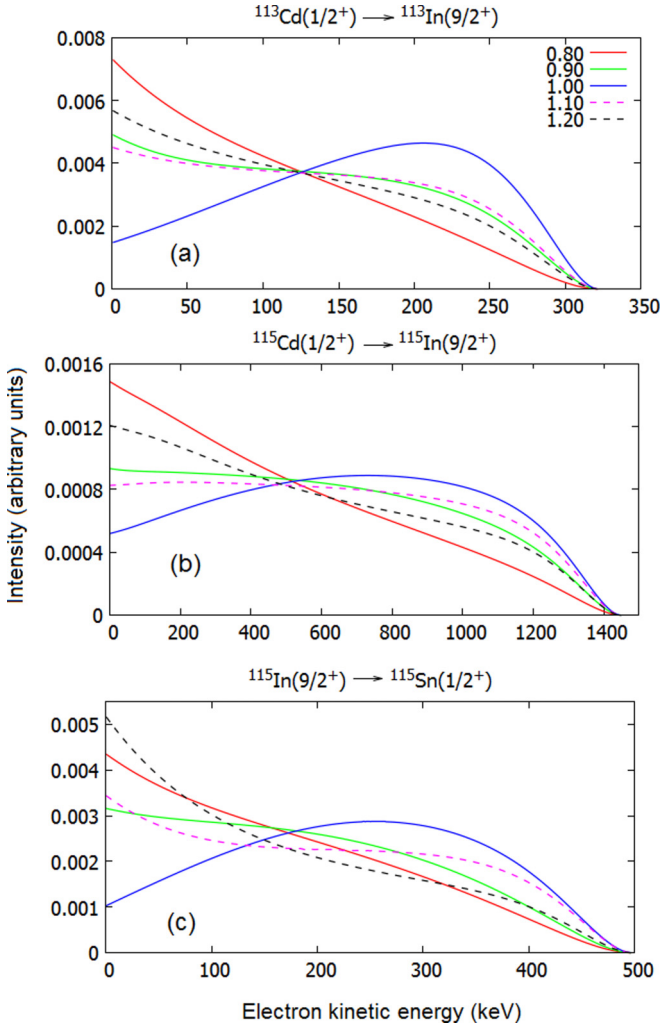

FIG. 7. The same as Fig. 2, but for the fourth-forbidden nonunique decays of ^{113}Cd, ^{115}Cd, and ^{115}In.

initial state to a $9/2^+$ final state. The decay of ^{87}Rb is experimentally measurable and thus another candidate for application of the spectrum-shape method. Unlike in the case of ^{99}Tc, the dependence is fairly simple: when g_A decreases, the low-energy intensity increases, and the intensity at larger energies decreases.

The results for fourth-forbidden decays, all nonunique, are presented in Figs. 7 and 8. The transitions are split into two groups according to their basic features. The first one consists of the decays of ^{113}Cd, ^{115}Cd, and ^{115}In shown in Fig. 7. The transitions of ^{113}Cd and ^{115}In are experimentally measurable and have been studied extensively (see Refs. [17,24,38,42]). The spectra show a distinctive hump when $g_A \approx g_V$. Interestingly, the behavior is similar to that of ^{99}Tc [see Fig. 5(c)]. These decays have one common feature: the $9/2^+$ state is either the initial or final state. For ^{113}Cd and ^{115}In the effect of varying the weak axial-vector coupling constant is in line with the results of Ref. [24]. However, in the earlier study [17] the turning point of the MQPM spectrum of ^{113}Cd was found to be at $g_A \approx 0.9$ and for ^{115}In at $g_A \approx 0.95$. It seems that the use of a larger model space for neutrons in this study and

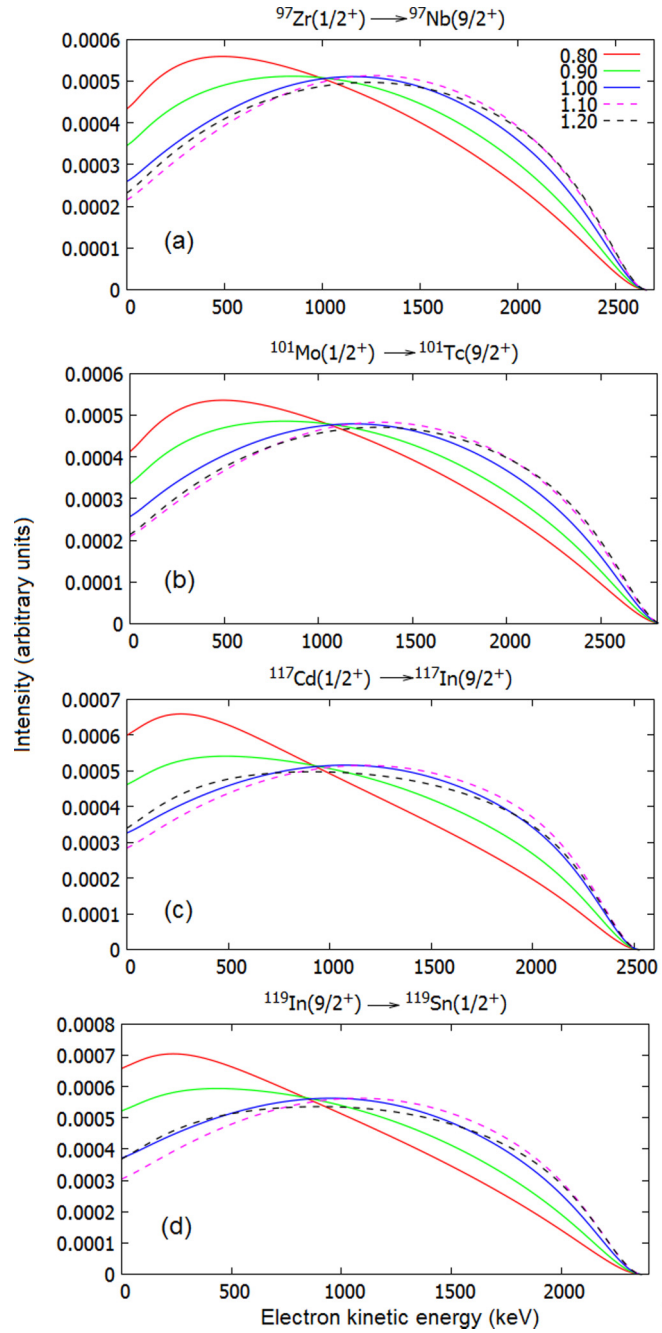

FIG. 8. The same as Fig. 2, but for the fourth-forbidden nonunique decays of ^{97}Zr, ^{101}Mo, ^{117}Cd, and ^{119}In.

in Ref. [24] has a notable effect on the shape of the electron spectrum. In Ref. [42] the electron spectra of these decays were calculated with the proton-neutron variant of MQPM with the free-nucleon values $g_V = 1.0$ and $g_A = 1.25$. The shapes of the resulting spectra are nearly identical, which further supports the results of this paper.

To see whether the strong dependence of the shape factor on the weak coupling constants of the fourth-forbidden nonunique decays is limited to the three neighboring nuclei, ^{113}Cd, ^{115}Cd, and ^{115}In, four further fourth-forbidden nonunique ground-state-to-ground-state transitions were studied. These were the

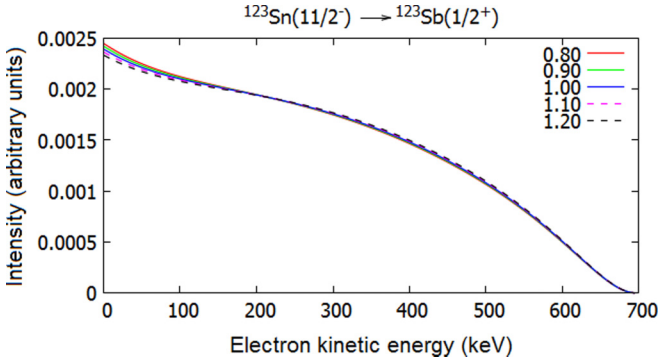

FIG. 9. The same as Fig. 2, but for the fifth-forbidden nonunique decay of ^{123}Sn.

ground-state-to-ground-state β^- decays of ^{97}Zr, ^{101}Mo, ^{117}Cd, and ^{119}Cd, for which the spectra are presented in Fig. 8. These four decays also behave almost identically as functions of g_A. For these decays the spectrum shape is rather similar when $g_A = 1.00$–1.20, but the shape changes radically when g_A is quenched below unity.

As shown thus far the dependence of the shape factor on the value of g_A seems to increase when the degree of forbiddeness grows. To test this hypothesis the fifth-forbidden decay of ^{123}Sn to the lowest $1/2^+$ excited state in ^{123}Sb (see Fig. 9) was included in this study. This transition is not experimentally measurable, but the theoretical results are important. As seen in the figure for this decay the spectrum shape does not depend on g_A in any significant way, thus invalidating the above-mentioned hypothesis. The sensitivity to g_A seems to connect more to the specific nuclear-structure details [like the almost magical involvement of a $9/2^+$ state in all the SSM-sensitive nuclei of Figs. 7, 8, and 5(c)] rather than to the forbiddeness of the decay transition.

The observation that the β spectra of many transitions behave similarly is a strong indication that significant changes in the MQPM-predicted level schemes do not affect the shape evolution of the β spectra. Similar conclusions can be drawn from Ref. [24] where the three nuclear models, MQPM, NSM, and IBFM-2 were used to study ^{113}Cd and ^{115}In decays. An obvious conclusion drawn from this is that the SSM seems to be quite insensitive to the fine details of the nuclear Hamiltonian and the different approximations adopted to solve the related eigenvalue problem. This makes the SSM very robust, and thus a reliable tool for determining the effective value of g_A.

B. Integrated shape factor $\tilde{C}$

In Refs. [17] and [24] it was noticed that for the decays of ^{113}Cd and ^{115}In the components $\tilde{C}_V$, $\tilde{C}_A$, and $\tilde{C}_{VA}$ of the decomposed integrated shape function $\tilde{C}$ [see Eq. (21)] have much larger absolute values than $\tilde{C}$. The integrated shape function and its components are listed in Table II for each of the presently studied transitions.

TABLE II. Unitless integrated shape functions $\tilde{C}$ of the studied transitions and their vector $\tilde{C}_V$, axial-vector $\tilde{C}_A$, and mixed components $\tilde{C}_{VA}$. For the total integrated shape factor $\tilde{C}$ the values of the coupling constants were set to $g_V = g_A = 1.0$.

Transition	Type	$\tilde{C}_V$	$\tilde{C}_A$	$\tilde{C}_{VA}$	$\tilde{C}$
^{125}Sb(7/2$^+$) → ^{125}Te(9/2$^-$)	1st non-uniq.	1.524×10^{-5}	4.734×10^{-6}	-1.428×10^{-5}	5.696×10^{-6}
^{141}Ce(7/2$^-$) → ^{141}Pr(5/2$^+$)	1st non-uniq.	1.906×10^{-1}	2.944×10^{-1}	-1.494×10^{-1}	7.069×10^{-2}
^{159}Gd(3/2$^-$) → ^{159}Tb(5/2$^+$)	1st non-uniq.	9.439×10^{-1}	2.436×10^{-1}	9.563×10^{-1}	2.144
^{161}Tb(3/2$^+$) → ^{161}Dy(5/2$^-$)	1st non-uniq.	7.937×10^{-3}	3.309×10^{-4}	-3.223×10^{-3}	5.045×10^{-3}
^{169}Er(1/2$^-$) → ^{169}Tm(3/2$^+$)	1st non-uniq.	1.833×10^{-2}	3.097×10^{-3}	-1.506×10^{-2}	6.369×10^{-3}
^{79}Se(7/2$^+$) → ^{79}Br(3/2$^-$)	1st unique	2.224×10^{-15}	1.161×10^{-12}	6.105×10^{-14}	1.224×10^{-12}
^{85}Kr(9/2$^+$) → ^{85}Rb(5/2$^-$)	1st unique	1.724×10^{-10}	2.540×10^{-5}	8.921×10^{-8}	2.549×10^{-5}
^{89}Sr(5/2$^+$) → ^{89}Y(1/2$^-$)	1st unique	2.219×10^{-16}	3.366×10^{-11}	1.233×10^{-13}	3.378×10^{-11}
^{107}Pd(5/2$^+$) → ^{107}Ag(1/2$^-$)	1st unique	8.332×10^{-17}	1.472×10^{-10}	6.432×10^{-14}	1.473×10^{-10}
^{125}Sb(7/2$^+$) → ^{125}Te(11/2$^-$)	1st unique	1.600×10^{-9}	1.397×10^{-4}	6.427×10^{-7}	1.404×10^{-4}
^{137}Cs(7/2$^+$) → ^{137}Ba(11/2$^-$)	1st unique	4.492×10^{-9}	3.311×10^{-4}	1.617×10^{-6}	3.328×10^{-4}
^{93}Zr(5/2$^+$) → ^{93}Nb(9/2$^+$)	2nd non-uniq.	2.020×10^{-16}	8.460×10^{-15}	-2.191×10^{-15}	6.471×10^{-15}
^{99}Tc(9/2$^+$) → ^{99}Ru(5/2$^+$)	2nd non-uniq.	4.342×10^{-9}	4.386×10^{-9}	-8.713×10^{-9}	1.602×10^{-11}
^{135}Cs(7/2$^+$) → ^{135}Ba(3/2$^+$)	2nd non-uniq.	1.133×10^{-8}	1.656×10^{-8}	2.737×10^{-8}	5.526×10^{-8}
^{137}Cs(7/2$^+$) → ^{137}Ba(3/2$^+$)	2nd non-uniq.	3.217×10^{-5}	2.654×10^{-5}	5.822×10^{-5}	1.169×10^{-4}
^{129}I(7/2$^+$) → ^{129}Xe(1/2$^+$)	2nd unique	8.191×10^{-22}	5.634×10^{-17}	2.685×10^{-19}	5.661×10^{-17}
^{85}Br(3/2$^-$) → ^{85}Kr(9/2$^+$)	3rd non-uniq.	1.597×10^{-6}	3.022×10^{-7}	-1.309×10^{-6}	5.902×10^{-7}
^{87}Rb(3/2$^-$) → ^{87}Sr(9/2$^+$)	3rd non-uniq.	1.531×10^{-13}	2.718×10^{-14}	-1.264×10^{-13}	5.387×10^{-14}
^{97}Zr(1/2$^+$) → ^{97}Nb(9/2$^+$)	4th non-uniq.	6.210×10^{-11}	4.995×10^{-11}	-1.055×10^{-10}	6.588×10^{-12}
^{101}Mo(1/2$^+$) → ^{101}Tc(9/2$^+$)	4th non-uniq.	8.370×10^{-11}	6.529×10^{-11}	-1.399×10^{-10}	9.131×10^{-12}
^{113}Cd(1/2$^+$) → ^{113}In(9/2$^+$)	4th non-uniq.	1.925×10^{-19}	2.094×10^{-19}	-4.002×10^{-19}	1.385×10^{-21}
^{115}Cd(1/2$^+$) → ^{115}In(9/2$^+$)	4th non-uniq.	2.030×10^{-14}	2.091×10^{-14}	-4.059×10^{-14}	6.238×10^{-16}
^{115}In(9/2$^+$) → ^{115}Sn(1/2$^+$)	4th non-uniq.	6.503×10^{-18}	6.126×10^{-18}	-1.256×10^{-17}	6.492×10^{-20}
^{117}Cd(1/2$^+$) → ^{117}In(9/2$^+$)	4th non-uniq.	7.361×10^{-12}	6.610×10^{-12}	-1.342×10^{-11}	5.545×10^{-13}
^{119}In(9/2$^+$) → ^{119}Sn(1/2$^+$)	4th non-uniq.	5.370×10^{-12}	4.441×10^{-12}	-9.441×10^{-12}	3.708×10^{-13}
^{123}Sn(11/2$^-$) → ^{123}Sb(1/2$^+$)	5th non-uniq.	3.791×10^{-28}	8.323×10^{-30}	-9.932×10^{-29}	2.881×10^{-28}

For all transitions the $\tilde{C}_{\rm V}$ and $\tilde{C}_{\rm A}$ components are positive, but the sign of $\tilde{C}_{\rm VA}$ varies. Although the next-to-leading-order terms are taken into account, $\tilde{C}$ is dominated by the axial-vector component in the unique decays. The vector and vector-axial components add small positive corrections, which are about two orders of magnitude smaller than $C_{\rm A}$ at their largest. For the nonunique first-forbidden decays the largest contribution comes from $\tilde{C}_{\rm V}$. The axial-vector component introduces a small positive correction, while the $\tilde{C}_{\rm VA}$ is negative, and has an absolute value of about 50%–90% of $\tilde{C}_{\rm V}$. As an exception, the $\tilde{C}_{\rm VA}$ component is positive for ^{159}Gd. The second-forbidden nonunique transitions on the other hand, have very different decompositions from each other. For ^{93}Zr the axial-vector component dominates, and the negative correction of $\tilde{C}_{\rm VA}$ is about 25%. In the case of ^{99}Tc, $\tilde{C}_{\rm V}$ and $\tilde{C}_{\rm A}$ have almost identical values, while $\tilde{C}_{\rm VA}$ is twice as large and negative. The resulting total integrated shape function $\tilde{C}$ is two orders of magnitude smaller than the absolute values of its components. For ^{135}Cs and ^{137}Cs the results are rather similar, but $\tilde{C}_{\rm VA}$ is positive. For the two third-forbidden nonunique decays the vector component dominates, the axial-vector component is small, and the absolute value of the negative $\tilde{C}_{\rm VA}$ is about 80% of the vector component. The fourth-forbidden decays are divided into the same groups as suggested by the electron spectra. The decomposition is similar to ^{99}Tc for ^{113}Cd, ^{115}Cd, and ^{115}In. For the rest of the fourth-forbidden decays $\tilde{C}_{\rm V}$ dominates, $\tilde{C}_{\rm A}$ is about 20% smaller, and $\tilde{C}_{\rm VA}$ is negative and has an absolute value of slightly less than the sum of $\tilde{C}_{\rm V}$ and $\tilde{C}_{\rm A}$. The resulting total integrated shape factor is one order of magnitude smaller than its components. For the fifth-forbidden transition of ^{123}Sn, $\tilde{C}$ is dominated by $\tilde{C}_{\rm V}$, and the corrections from other components are small.

V. CONCLUSIONS

The sensitivity of the shapes of electron spectra for 26 forbidden β^- decays of odd-A nuclei were studied by using the nuclear matrix elements derived from the microscopic quasiparticle-phonon model (MQPM) and by varying the value of the axial-vector coupling constant $g_{\rm A}$. The next-to-leading-order terms were included in the corresponding β-decay shape factors. In the spectrum-shape method (SSM) the shapes of computed electron spectra can be compared with the measured ones to access the effective value of $g_{\rm A}$. The shape of the computed electron spectrum was found to be unaffected by minor changes in the computed excitation spectra of the involved nuclei, implying stability against the variations of the details of the nuclear Hamiltonian. This is supported by the study [24] where three different nuclear Hamiltonians were used. The study of Ref. [24] suggests also that the SSM is not very sensitive to the many-body framework used to solve the Hamiltonian-related eigenvalue problem since the three nuclear-structure models produced quite compatible SSM results despite their completely different theory frameworks. At the level of the mean field, in turn, in most cases moving the single-particle energies of the underlying mean field by as much as 1.5 MeV did not affect the normalized β spectra, even though the half-life was affected significantly. Furthermore, transitions of the same type (forbiddeness, uniqueness) in neighboring nuclei produce similar spectrum shapes regardless of the Q value. The above features make the SSM a much more robust method than just comparing the theoretical and experimental half-lives to extract the effective value of $g_{\rm A}$.

The electron spectrum of the ground-state-to-ground-state decays of ^{99}Tc and ^{87}Rb depend significantly on the effective value of the axial-vector coupling constant $g_{\rm A}$. Since these decays are experimentally measurable, they can be used to gain knowledge on the effective value of $g_{\rm A}$ in second- and third-forbidden nonunique beta decays by using the spectrum-shape method. The decays for which the spectrum shape does not depend on the values of the weak coupling constants, such as the transitions of ^{135}Cs and ^{137}Cs, could be used to test the accuracy of the theoretical spectra.

The shape factors of the third- and especially fourth-forbidden decays depend very sensitively on the value of the coupling constants. Besides the transitions in this study, there are no other medium-heavy odd-A nuclei which have a third- or fourth-forbidden decay branch with a significant branching ratio. However, for example ^{50}V decays via a fourth-forbidden nonunique transition and could be a candidate for SSM when a shell-model type of framework would be used to evaluate the needed wave functions.

In general, the decomposition of the integrated shape functions $\tilde{C}$ into vector, axial-vector, and vector-axial-vector components is similar when the normalized β spectra resemble each other. However, the decompositions of the studied first- and third-forbidden nonunique decays are similar, with the exception of the one of ^{159}Gd, but the normalized β spectra of these decays are nothing alike.

Finally, the information gained through SSM on the effective value of $g_{\rm A}$ in forbidden decay transitions could help in solving the $g_{\rm A}$ problem related to the neutrinoless double beta decay, which proceeds via virtual transitions, and largely via the forbidden ones.

ACKNOWLEDGMENTS

This work has been partially supported by the Academy of Finland under the Finnish Centre of Excellence Programme 2012-2017 (Nuclear and Accelerator Based Programme at JYFL).

[1] J. Suhonen and O. Civitarese, Phys. Rep. **300**, 123 (1998).
[2] J. Maalampi and J. Suhonen, Adv. High Energy Phys. **2013**, 505874 (2013).
[3] H. Ejiri, N. Soukouti, and J. Suhonen, Phys. Lett. B **729**, 27 (2014).
[4] H. Ejiri and J. Suhonen, J. Phys. G **42**, 055201 (2015).

[5] R. P. Feynmann and M. Gell-Mann, Phys. Rev. **109**, 193 (1958).
[6] R. P. Feynmann and M. Gell-Mann, Phys. Rev. **111**, 362 (1958).
[7] W. Theis, Eur. Phys. J. A **150**, 590 (1958).
[8] K. Zuber, *Neutrino Physics* (Institute of Physics Publishing, Ltd., London, 2004).
[9] E. D. Commins, *Weak Interactions* (McGraw-Hill, New York, 2007).
[10] J. Suhonen, *From Nucleons to Nucleus: Concepts of Microscopic Nuclear Theory* (Springer, Berlin, 2007).
[11] J. Suhonen and O. Civitarese, Phys. Lett. B **725**, 153 (2013).
[12] J. Suhonen and O. Civitarese, Nucl. Phys. A **924**, 1 (2014).
[13] P. Pirinen and J. Suhonen, Phys. Rev. C **91**, 054309 (2015).
[14] D. S. Delion and J. Suhonen, Europhys. Lett. **107**, 52001 (2014).
[15] F. F. Deppisch and J. Suhonen, Phys. Rev. C **94**, 055501 (2016).
[16] J. Kostensalo and J. Suhonen, Phys. Rev. C **95**, 014322 (2017).
[17] M. Haaranen, P. C. Srivastava, and J. Suhonen, Phys. Rev. C **93**, 034308 (2016).
[18] J. Toivanen and J. Suhonen, J. Phys. G **21**, 1491 (1995).
[19] J. Toivanen and J. Suhonen, Phys. Rev. C **57**, 1237 (1998).
[20] B. H. Wildenthal, M. S. Curtin, and B. A. Brown, Phys. Rev. C **28**, 1343 (1983).
[21] G. Martínez-Pinedo, A. Poves, E. Caurier, and A. P. Zuker, Phys. Rev. C **53**, R2602(R) (1996).
[22] E. Caurier, F. Nowacki, and A. Poves, Phys. Lett. B **711**, 62 (2012).
[23] P. Belli, R. Bernabei, N. Bukilic, F. Cappella, R. Cerulli, C. J. Dai, F. A. Danevich, J. R. de Laeter, A. Incicchitti, V. V. Kobychev, S. S. Nagorny, S. Nisi, F. Nozzoli, D. V. Poda, D. Prosperi, V. I. Tretyak, and S. S. Yurchenko, Phys. Rev. C **76**, 064603 (2007).
[24] M. Haaranen, J. Kotila, and J. Suhonen, Phys. Rev. C **95**, 024327 (2017).
[25] F. Iachello and A. Arima, *The Interacting Boson Model* (Cambridge University Press, Cambridge, 1987).
[26] F. Iachello and P. V. Isacker, *The Interacting Boson-Fermion Model* (Cambridge University Press, USA, 1991).
[27] H. Behrens and W. Bühring, *Electron Radial Wave Functions and Nuclear Beta Decay* (Clarendon, Oxford, 1982).
[28] M. Baranger, Phys. Rev. **120**, 957 (1960).
[29] A. Bohr, B. R. Mottelson, and D. Pines, Phys. Rev. **110**, 936 (1958).
[30] N. N. Bogoliubov, Sov. Phys. JETP **34**, 41 (1958).
[31] J. Valatin, Phys. Rev. **122**, 1012 (1961).
[32] P. Ring and P. Schuck, *The Nuclear Many-Body Problem* (Springer, New York, 1980).
[33] G. Audi and A. Vapstra, Nucl. Phys. A **565**, 1 (1993).
[34] G. Audi and A. Vapstra, Nucl. Phys. A **595**, 409 (1995).
[35] D. Rowe, *Nuclear Collective Motion* (Methuen, London, 1970).
[36] National Nuclear Data Center, Brookhaven National Laboratory, www.nndc.bnl.gov.
[37] J. C. Hardy, I. S. Towner, V. Koslowsky, E. Hagberg, and H. Schmeing, Nucl. Phys. A **509**, 429 (1990).
[38] M. T. Mustonen, M. Aunola, and J. Suhonen, Phys. Rev. C **73**, 054301 (2006).
[39] M. Haaranen and J. Suhonen, Eur. Phys. J. A **19**, 93 (2013).
[40] A. Bohr and B. R. Mottelson, *Nuclear Structure* (Benjamin, New York, 1969), Vol. I.
[41] G. Audi, F. G. Kondev, M. Wang, B. Pfeiffer, X. Sun, J. Blachot, and M. MacCormick, Chin. Phys. C **36**, 1157 (2012).
[42] M. T. Mustonen and J. Suhonen, Phys. Lett. B **657**, 38 (2007).